

Deciphering the Structural Properties That Confer Stability to a DNA Nanocage

Mattia Falconi,^{†,*} Francesco Oteri,[†] Giovanni Chillemi,[§] Felicie F. Andersen,^{||} David Tordrup,^{||} Cristiano L. P. Oliveira,^{||} Jan S. Pedersen,^{||} Birgitta R. Knudsen,^{||} and Alessandro Desideri^{†,*}

[†]Department of Biology and Center of Biostatistics and Bioinformatics, University of Rome "Tor Vergata", Via della Ricerca Scientifica 1, 00133 Rome, Italy, [‡]NAST Nanoscience & Nanotechnology & Innovative Instrumentation, University of Rome "Tor Vergata", Via della Ricerca Scientifica 1, 00133 Rome, Italy, [§]CASPUR Inter-University Consortium for the Application of Super-Computing for Universities and Research, Via dei Tizii 6, Rome 00185, Italy, ^{||}Department of Molecular Biology and Interdisciplinary Nanoscience Center (iNANO), Aarhus University, C.F. Møllers Allé, Bldg. 130, 8000 Aarhus C, Denmark, and [¶]Department of Chemistry and Interdisciplinary Nanoscience Center (iNANO), Aarhus University, Langelandsgade 140, 8000 Aarhus C, Denmark

Intermolecular interactions of DNA are highly specific and readily programmable through Watson–Crick complementarity. This complementarity, together with its high chemical and physical stability, can be used to design systems in which single strands self-assemble from double strands to more complex motifs. For this reason, the DNA strands represent the ideal molecule for the design of self-assembling structures.^{1–5} Successful strategies for synthesis of simple synthetic DNA substrates to be used for enzyme analyses,^{6–8} as well as more complex 2D DNA structures for both scientific and technological purposes, have been presented.^{9–13} Assembly of 3D DNA structures, however, has proven more difficult,^{14–19} and a better understanding of the behavior of DNA structures in 3D is necessary for future progress. Seeman and co-workers^{14,15} have been the first to complete the building of a cube and a truncated octahedron DNA structure, although these were hampered by a low yield of about 1%. Later, an octahedron was elegantly folded with high yield from a single DNA fragment by the Joyce group.¹⁶ The design of this structure, however, compromised the possibilities for covalent closure. Goodman and co-workers¹⁷ have synthesized tetrahedrons characterized by both high yield (95%) and covalent closure, and an elegant new approach of using relatively simple building blocks for the efficient assembly of more complex 3D structures including cubic, pentagonal, and hexagonal prisms was presented by Aldaye and Sleiman.¹⁹

Recently, a covalently closed and efficiently assembled 3D DNA structure with a

ABSTRACT A DNA nanocage has been recently characterized by small-angle X-ray scattering (SAXS) and cryo-transmission electron microscopy as a DNA octahedron having a central cavity larger than the apertures in the surrounding DNA lattice. Starting from the SAXS data, a DNA nanocage has been modeled and simulated by classical molecular dynamics to evaluate *in silico* its structural properties and stability. Global properties, principal component analysis, and DNA geometrical parameters, calculated along the entire trajectory, indicate that the cage is stable and that the B-DNA conformation, also if slightly distorted, is maintained for all the simulation time. Starting from the initial model, the nanocage scaffold undergoes a contraction of the thymidine strands, connecting the DNA double helices, suggesting that the length of the thymidine strands is a crucial aspect in the modulation of the nanocage stability. A comparison of the average structure as obtained from the simulation shows good agreement with the SAXS experimental data.

KEYWORDS: molecular dynamics simulation · SAXS spectroscopy · DNA nanocage structure · DNA flexibility and geometrical parameters · principal component analysis

complexity exceeding that of the tetrahedron presented by Goodman and co-workers¹⁷ has been produced.²⁰ This structure is built from eight oligonucleotides and has the connectivity of an octahedron as defined by its double-stranded regions (Figure 1A,B). The structure has the form of a DNA cage composed of an outer lattice with apertures smaller in diameter than the central spherical cavity, as confirmed by cryo-transmission electron microscopy (cryo-TEM) and small-angle X-ray scattering (SAXS).²⁰ The structure and stability of DNA nanostructures can be useful probed by molecular dynamics (MD) simulations, as shown in the case of paranemic crossovers^{21–23} and nanocircles.^{24,25}

In this paper, an MD simulation of the octahedron nanocage has been carried out with the aim of understanding the rules that confer stability to this complex DNA nanostructure. Analyses indicate that the B-DNA

*Address correspondence to desideri@uniroma2.it.

Received for review May 7, 2009 and accepted June 15, 2009.

Published online June 22, 2009.
10.1021/nn900468y CCC: \$40.75

© 2009 American Chemical Society

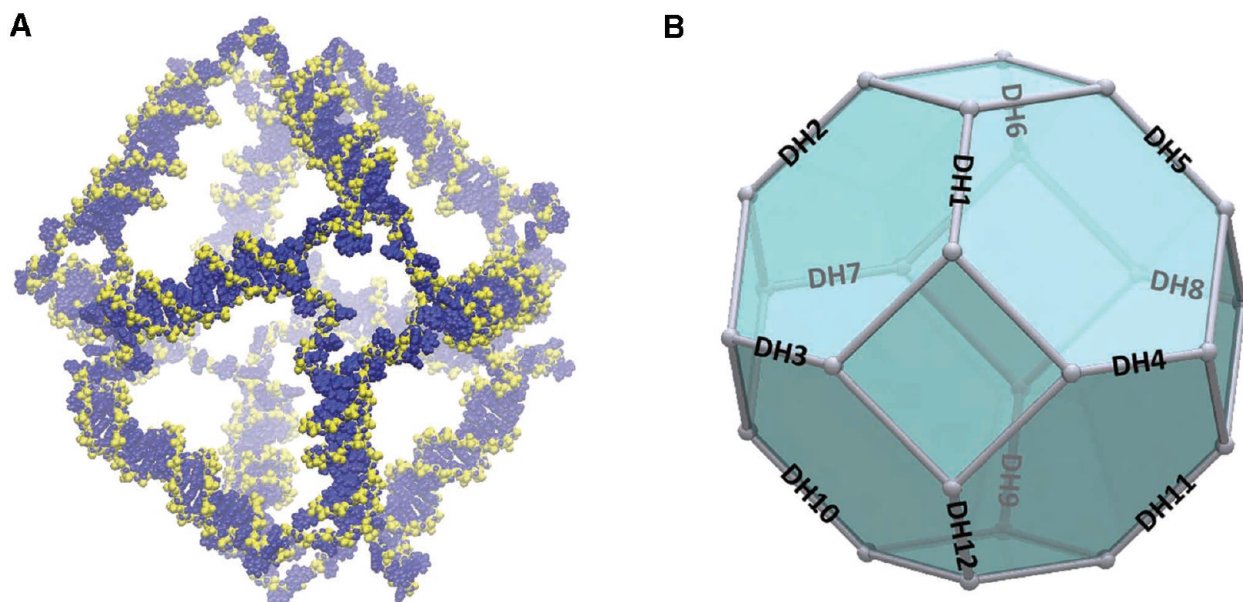


Figure 1. (A) View of the DNA nanocage starting structure. The nucleotides are shown in blue, while the sugar–phosphate backbone is represented in yellow. The picture was produced using the VMD program.⁴⁵ (B) Schematic view of the truncated octahedron geometry of the DNA nanocage highlighting the 12 DNA double helices (from DH1 to DH12). The edges of the square polyhedron faces represent the thymidine strands.

double helix structure is maintained in spite of a change in the helix axis curvature. Furthermore, a key role is observed for the thymidine strands that, assembling through hydrophobic interactions, induce a nanocage contraction.

RESULTS

Root Mean Square Deviations and Fluctuations. Figure 2 represents the all-atoms rmsd, from the starting structure as a function of time, for the entire nanocage structure (black), for all the double helices (dark gray), and for all the thymidine strands (light gray). The rmsd values reach a stable value within the first nanosecond (Figure 2), with the double helices being more stable than the thymidine strands. The stability of the nanocage

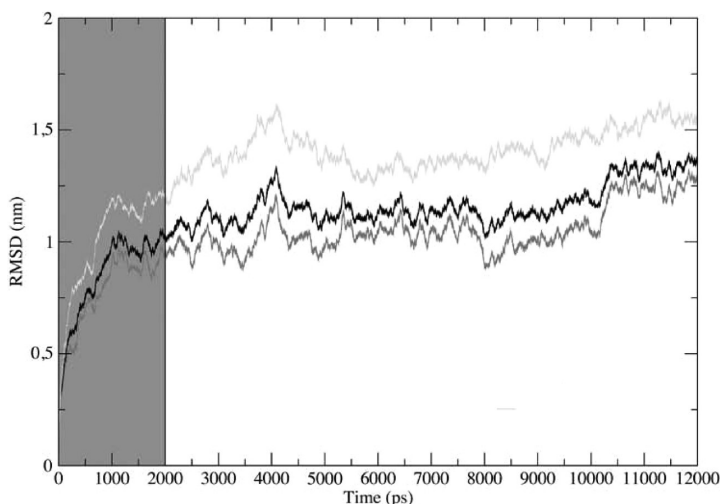


Figure 2. DNA nanocage rmsd from starting structure of all atoms (black), DNA double helices (dark gray), and thymidine strands (light gray). The gray box indicates the trajectory fraction not considered in the analyses.

structure is confirmed also by the time evolution of the gyration radius (Figure 3) that assumes an average value of 6.5 nm ($SD \pm 0.03$) and confirms the high stability of the double helices. In line, the rmsd of each single double helix oscillates between 0.2 and 0.4 nm (Figure 1 of Supporting Information) and that of the thymidine strands between 0.2 and 0.8 nm (Figure 2 of Supporting Information), indicating that the unstructured thymidine strands undergo a larger deviation from the initial structure.

All of the following analyses were carried out over the last 10 ns to guarantee an investigation over a well-thermalized system. The rmsf values averaged over each nucleotide of the DNA strands maintain values under 0.3 nm, excluding the 3' and the 5' base pairs directly connected with the thymidine single strand (Figure 3 of Supporting Information), confirming the stability of DNA double helices in the nanocage structure. The thymidine strands reach rmsf values up to 0.4 nm (Figure 4 of Supporting Information) and can be considered as flexible connectors of the stable double helices.

DNA Geometrical Analysis. All of the geometrical parameters that characterize the standard B-DNA have been monitored and averaged along the trajectory to accurately analyze each possible geometrical deformation of the 12 DNA double helices.

The average values with their standard deviations are shown in Tables 1 and 2, in comparison with the standard B-DNA geometrical parameters. The averaged calculated parameters are close to the typical B-DNA geometrical parameters, indicating a good stability and a regular geometry of the double helices that is maintained over all the simu-

lation time. In DH9, two nucleotides are locally unfolded at the connection with the thymidine bridge DH7–9 that, duplicating its buried surface (Figure 5), exceptionally steers one extremity of DH9. These nucleotides have been excluded from the calculations shown in Tables 1 and 2. The slide parameter (first column of Table 1 in the lower panel) that in all of the helices reaches an average value of 3.4 Å, against the 0 value typical of a standard B-DNA, determines the slight double helix curvature (of about 30°) occurring in each helix (Table 2).

Principal Component Analysis. The principal component analysis (PCA), or essential dynamics,²⁶ has been applied to the nanocage trajectory. The analysis is based on the diagonalization of the covariance matrix, built from the atomic fluctuations after the removal of the translations and rotations by fitting the trajectory on the first structure saved after the thermalization phase, and permits the identification of the main 3N directions (eigenvectors) along which the majority of the motion is defined. The analysis, carried out on the phos-

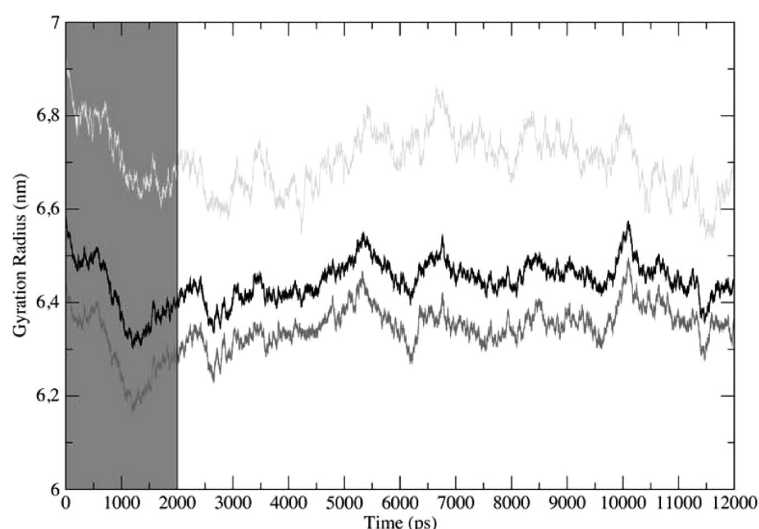


Figure 3. Time evolution of the DNA nanocage gyration radius of all atoms (black), DNA double helices (dark gray), and thymidine strands (light gray). The gray box indicates the trajectory fraction not considered in the analyses.

phorus atoms of the DNA backbone,²⁷ indicates that the motion is dispersed over 1800 eigenvectors, but about 90% of the motion depends on the first 20 eigen-

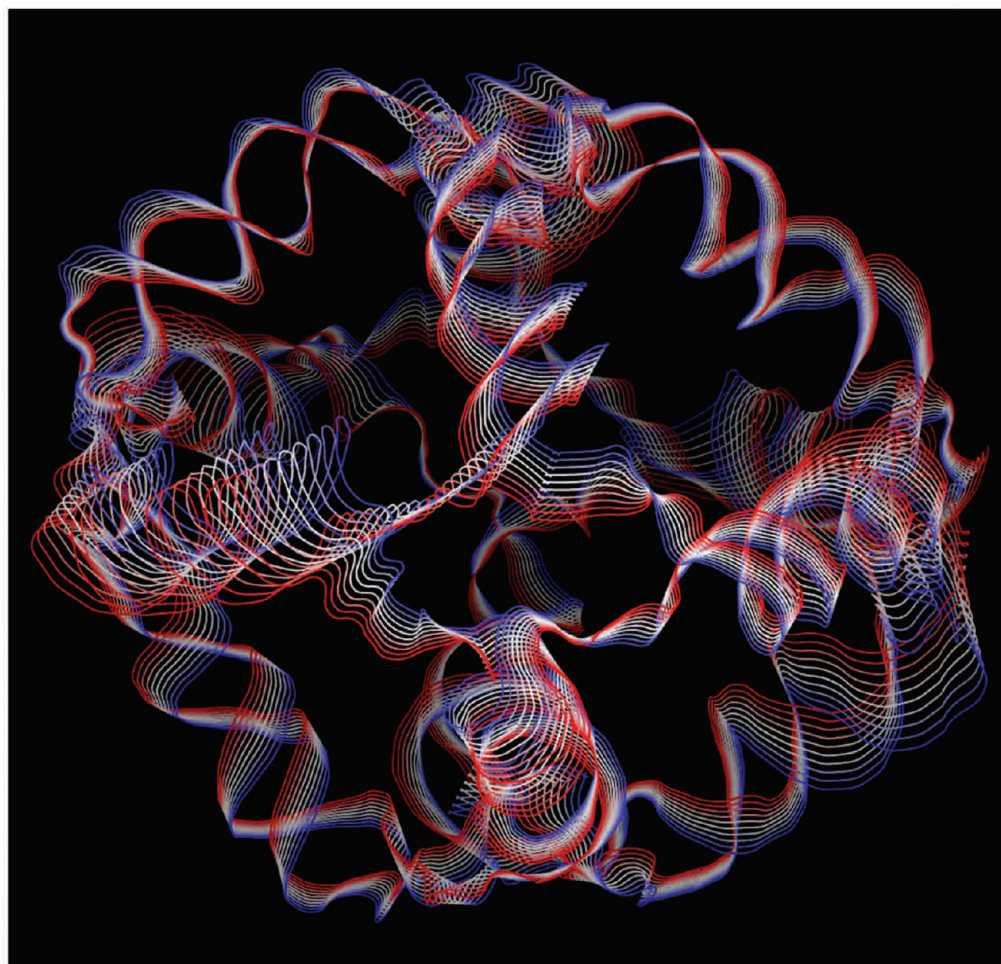
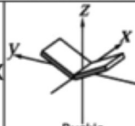
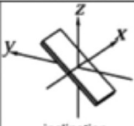
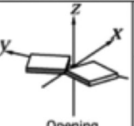
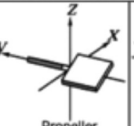
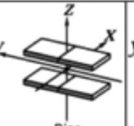
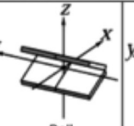
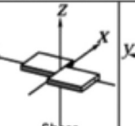
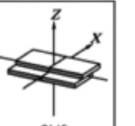
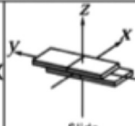
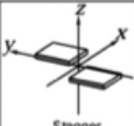
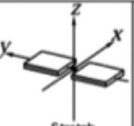
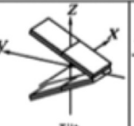
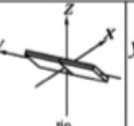
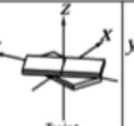
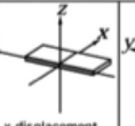
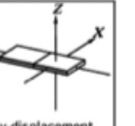


Figure 4. Tube representation of the motion projections along the first eigenvector for the nanocage structure. The width of the ribbon, generated by the flanking tubes, indicates the amplitude of the motion, the direction going from the red to the blue. This picture was produced using the VMD program.⁴⁵

TABLE 1. DNA Parameters of the 12 DNA Double Helices Compared with the Standard B-DNA Values (Standard Deviations are Indicated in Parentheses)

DNA Helix								
B-DNA	0.00	2.74	0.16	-15.07	3.38	0.00	0.00	0.00
DH1	1.52 (13.38)	0.06 (3.43)	3.58 (2.61)	-11.31 (6.27)	3.53 (6.16)	0.45 (3.16)	0.02 (0.27)	-0.01 (0.42)
DH2	-0.83 (4.75)	-1.43 (1.23)	2.70 (1.03)	-8.50 (8.34)	3.73 (6.12)	-0.14 (2.58)	-0.01 (0.14)	0.02 (0.52)
DH3	0.19 (8.11)	-3.43 (2.56)	2.89 (3.16)	-8.82 (5.34)	4.77 (6.98)	-0.00 (2.12)	-0.02 (0.15)	0.00 (0.38)
DH4	-0.89 (6.87)	-2.48 (2.25)	2.72 (1.62)	-10.19 (5.79)	3.90 (6.18)	0.28 (1.96)	-0.01 (0.16)	0.03 (0.25)
DH5	0.52 (8.29)	-2.89 (1.28)	3.19 (1.79)	-9.16 (6.56)	4.00 (5.20)	-0.01 (2.19)	-0.01 (0.15)	-0.03 (0.42)
DH6	0.14 (6.16)	-2.15 (1.44)	2.87 (2.25)	-9.14 (8.25)	4.70 (6.58)	0.08 (2.57)	0.03 (0.15)	-0.02 (0.44)
DH7	-1.38 (7.56)	-0.61 (4.53)	2.80 (1.48)	-9.27 (7.49)	3.74 (6.77)	-0.03 (3.59)	0.03 (0.14)	-0.02 (0.39)
DH8	-0.79 (7.69)	-2.86 (2.26)	2.89 (1.46)	-9.55 (7.39)	3.98 (5.65)	-0.39 (2.46)	-0.00 (0.18)	-0.02 (0.41)
DH9	-1.81 (8.24)	-2.22 (4.51)	3.51 (1.29)	-7.65 (8.54)	3.97 (5.46)	1.03 (2.52)	-0.02 (0.15)	0.04 (0.50)
DH10	0.27 (8.94)	0.70 (4.30)	3.21 (1.91)	-8.76 (8.50)	4.07 (7.14)	0.43 (3.38)	0.00 (0.18)	0.03 (0.38)
DH11	-0.86 (5.67)	-1.66 (2.20)	2.95 (1.56)	-8.79 (6.86)	4.67 (6.25)	0.37 (2.76)	-0.01 (0.14)	0.00 (0.42)
DH12	-0.64 (6.52)	-2.88 (1.54)	3.04 (1.85)	-8.65 (6.55)	4.37 (7.34)	0.11 (2.84)	0.00 (0.14)	0.03 (0.47)
Average	-0.38	-1.82	3.03	-9.15	4.12	0.18	0.00	0.01

DNA Helix								
B-DNA	0.00	-0.09	0.01	0.00	0.00	36.00	0.18	0.00
DH1	3.45 (0.33)	-0.16 (0.32)	0.22 (0.11)	-0.16 (0.35)	1.78 (2.81)	33.51 (4.79)	-1.13 (0.19)	-0.01 (0.28)
DH2	3.41 (0.17)	-0.08 (0.11)	0.17 (0.02)	-0.14 (0.24)	-0.92 (3.00)	33.25 (3.27)	-0.74 (0.17)	0.01 (0.29)
DH3	3.42 (0.30)	-0.02 (0.11)	0.16 (0.04)	-0.13 (0.36)	0.07 (2.28)	31.66 (5.94)	-0.64 (0.17)	-0.02 (0.23)
DH4	3.39 (0.22)	-0.02 (0.20)	0.17 (0.03)	-0.10 (0.24)	1.09 (3.48)	33.38 (3.49)	-0.62 (0.15)	-0.04 (0.22)
DH5	3.42 (0.28)	-0.04 (0.12)	0.18 (0.03)	-0.13 (0.28)	0.55 (3.20)	33.58 (3.88)	-0.78 (0.15)	-0.01 (0.25)
DH6	3.40 (0.23)	-0.06 (0.17)	0.17 (0.03)	-0.16 (0.31)	0.05 (3.08)	32.06 (6.69)	-0.59 (0.18)	0.01 (0.31)
DH7	3.38 (0.23)	-0.05 (0.17)	0.18 (0.03)	-0.15 (0.37)	-0.05 (3.48)	33.04 (3.90)	-0.67 (0.17)	-0.06 (0.48)
DH8	3.41 (0.22)	-0.00 (0.13)	0.17 (0.03)	-0.11 (0.22)	-0.74 (2.94)	33.32 (4.23)	-0.54 (0.20)	0.02 (0.22)
DH9	3.46 (0.27)	-0.05 (0.20)	0.17 (0.04)	-0.16 (0.28)	1.90 (2.80)	33.25 (2.15)	-0.73 (0.22)	-0.23 (0.36)
DH10	3.35 (0.26)	-0.05 (0.21)	0.19 (0.03)	-0.16 (0.29)	0.08 (3.99)	32.76 (3.84)	-0.75 (0.17)	-0.06 (0.48)
DH11	3.39 (0.16)	-0.07 (0.11)	0.18 (0.02)	-0.09 (0.26)	0.41 (4.72)	32.86 (3.70)	-0.57 (0.16)	-0.03 (0.22)
DH12	3.40 (0.22)	-0.03 (0.13)	0.17 (0.03)	-0.13 (0.23)	-0.30 (3.24)	32.96 (3.32)	-0.69 (0.19)	-0.02 (0.26)
Average	-0.38	-1.82	3.03	-9.15	4.12	0.18	0.00	0.01

vectors (Figure 5 of Supporting Information), while the three graphs showing the projections of the first, second, and third principal components are shown in Figure 6 of the Supporting Information, as usually found in many different systems.^{27–29} The convergence of the simulations has been probed measuring the cosine content of the first principal component that shows a value of 0.004, indicating a good convergence of the simulation.³⁰

Projection of the phosphorus atoms along the first eigenvector, which contain about 50% of the total motion (Figure 5 of Supporting Information), permits one to describe the main component of the motion as depicted by the cage reported in Figure 4, where the width of the ribbon is proportional to the amplitude of the motion, the direction going from the red to the blue. The nanocage shows a distinctive motion generated by two main features: the stacking of the thymi-

dine hydrophobic rings and the rotation of the double helices. The thymidine rings, connecting the DNA double helices, stack to maximize their hydrophobic interactions, inducing a reduction of the strand length and a variable rotation/inclination of each double helix composing the nanocage. The rotation of the double helix occurs over an axis parallel to the central axis and tangent to the DNA backbone (Supporting Information movie file).

The stacking of the thymidine rings can be appreciated for each thymidine strand by plotting the buried surface of the hydrophobic rings averaged over the MD trajectory, compared to the same surfaces in the starting model. The buried surface of every thymidine strand is about 500 Å² in the starting nanocage structure (Figure 5 black bars) and becomes about 600 Å² during the MD simulation (Figure 5 dot-filled bars). The thymidines in the bridge can aggregate with different orienta-

tions, generating a hidden surface of different sizes that summed together generate the observed buried surface increase.

The rotational motion of the double helices can be appreciated by calculating for each helix the rmsf of each nucleotide over the direction of the first eigenvector (Figure 6). For each helix strand, the rmsf has a sinusoidal trend. The nucleotides close to the rotation axis, which differs in position and inclination compared to the helix axis, are characterized by a low fluctuation value and the nucleotides far from this axis by a large fluctuation value.

Single Elements Cross Correlations. Interesting results concerning the relative flexibility and communication of the nanocage can be obtained by looking at the correlated motions between different strand regions of the nanocage. A correlation map³¹ has been calculated measuring the average correlation over the entire thymidine strands and the entire single strands forming the double helices considered as independent elements (inset of Figure 7). In the map (Figure 7), a spot represents a correlation between two elements whose intensity follows the colored scale depicted in the figure.

The map shows three kinds of correlation: (I) large squares representing correlations between two single strands composing a double helix; (II) small squares representing correlations between two different thymidine strands; (III) rectangles representing correlations between a thymidine strand *versus* any double helix single strand.

The gray spots represent positive correlations between elements, close in the nanocage structure because covalently or non-covalently linked, that move in the same direction. The cyan spots describe negative correlations between two far away elements, such as two thymidine strands (cyan small square spots) or a thymidine strand and the single double helix strand (cyan rectangular spots).

The negative correlations are the most interesting ones since they occur between elements located far away and indicate that the cage is contracting, in agreement with the nanocage motion described by the first eigenvector (Figure 4, and Supporting Information movie file) and the increment of thymidine strand buried surface (Figure 5).

Comparison of the MD Model with Small-Angle Scattering Data. For the comparison with the SAXS data, 20 configurations have been extracted from the trajectory with a time step of 0.5 ns. The theoretical intensity and pair distance distribution function, $p(r)$, which is a histogram of pair distances inside of the particle,

TABLE 2. Curvature Degree of the 12 DNA Double Helices Compared with the Standard B-DNA Values^a

DNA Helix	Sequence	
B-DNA		0.0
DH1	CGATGTCTAAGCTGACCG	17.48 (8.71)
DH2	GGACCGTGATTCCATGAC	33.89 (12.46)
DH3	CTTAGAGTTGCCACCAGG	50.31 (15.57)
DH4	GAATCCTATGCTCGGACG	24.41 (11.43)
DH5	GGCTCACATTGGCTACAG	25.65 (11.05)
DH6	CTATCCGATCGAGGCATG	28.72 (12.16)
DH7	CATACTGAGAGCGTTCCG	19.26 (9.28)
DH8	GTCGCAGTTCAGATACGC	33.21 (13.08)
DH9	CGTTACGGTACAATGCC	30.87 (14.70)
DH10	CGCAAGACGTTAGTGCC	35.17 (13.74)
DH11	CCACCGAATGGTGTATCG	24.34 (11.79)
DH12	GTATGACGCAGCACTTGC	35.41 (13.97)
Average(SD)		12.5 (2.16)

^aThe central column indicates the sequence of one strand. The standard deviations are indicated in parentheses.

for each model is shown in Figure 8. The intensities and $p(r)$ functions are very similar for the 20 models, which shows that the fluctuations in the simulations induce only small changes in the theoretical scattering intensities and $p(r)$ functions. On the basis of this result,

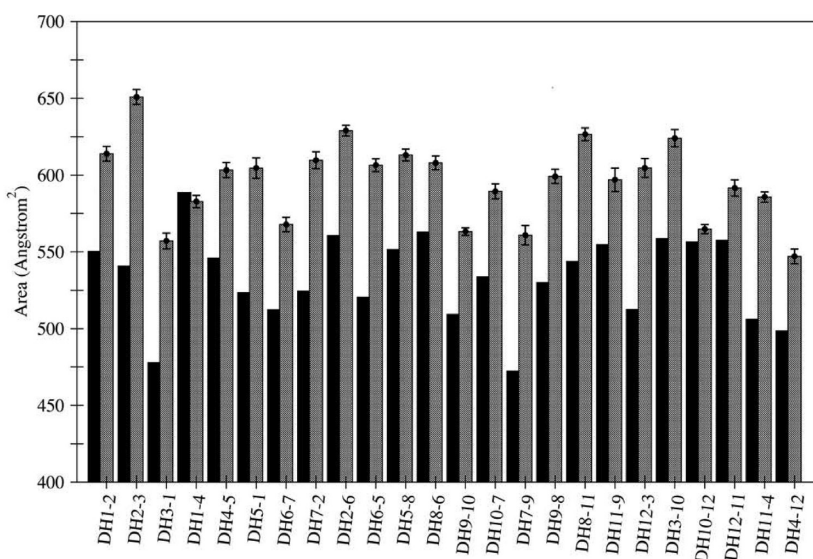


Figure 5. Histogram representing the buried hydrophobic surface of each thymidine strand averaged over the trajectory (dot-filled bar) compared to the starting value (black bar). The standard deviation is reported at the top of each MD bar.

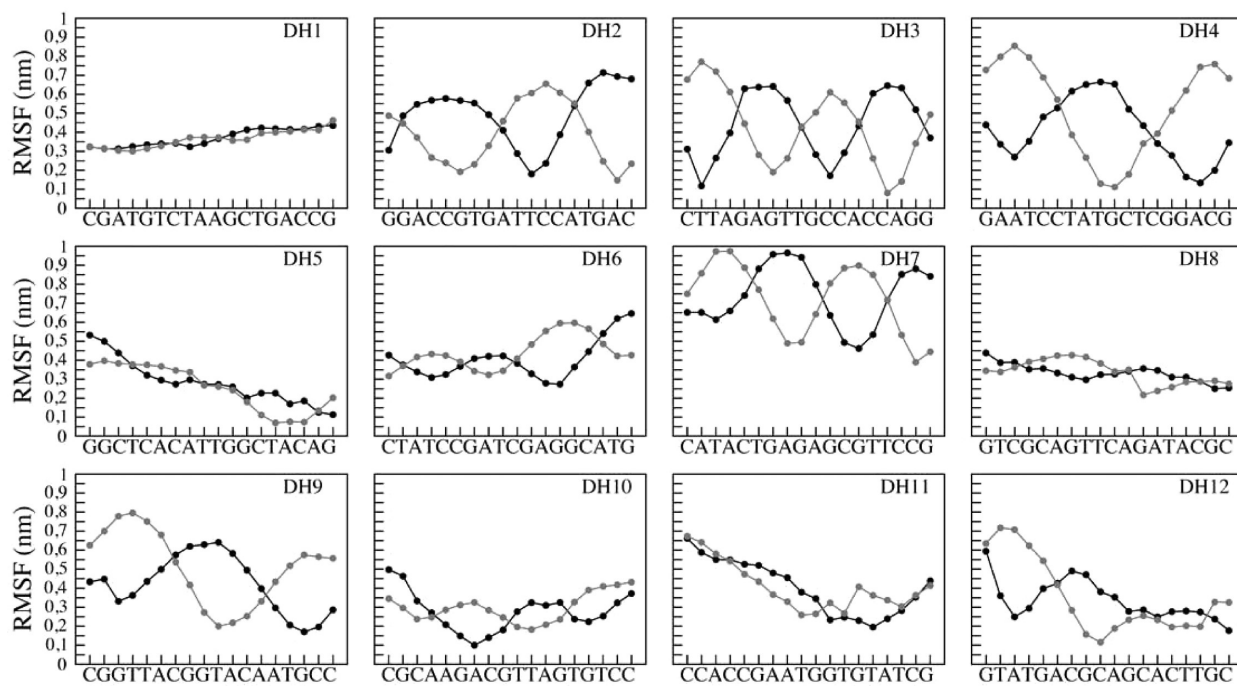


Figure 6. Average per nucleotide rmsf for each of the two strands of the 12 DNA double helices (from DH1 to DH12), calculated over the first eigenvector. Black and gray filled circles indicate the two strand nucleotides. The DNA sequence of each double helix is shown in the lower side of each panel.

it is a reasonable approximation to use the average scattering intensity (solid line in Figure 8) for the comparison with experimental results.

The inset of Figure 8 displays the radius of gyration R_G and maximum particle dimension D_{MAX} for each con-

figuration extracted from the simulation. The averaged values, $R_G = 6.47 \pm 0.04$ nm and $D_{MAX} = 16.2 \pm 0.3$ nm, are in good agreement with the ones obtained from the experimental data: $R_G = 6.7 \pm 0.3$ nm and $D_{MAX} \sim 16.5$ nm.²⁰

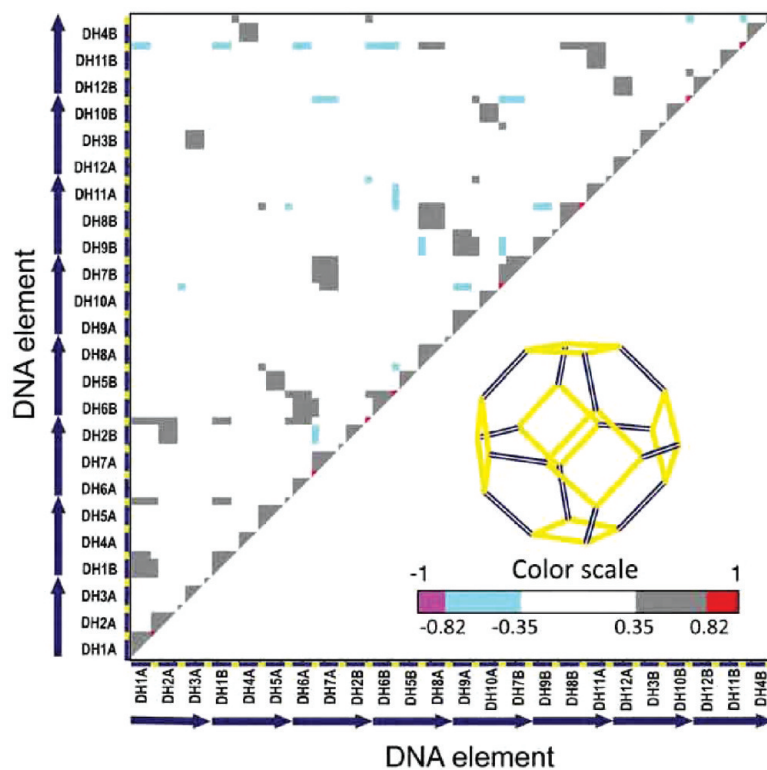


Figure 7. Correlation map for the nanocage DNA single-strand elements represented by blue bars (double helix strand) and yellow bars (thymidine strand). These strands are also shown in the inset representing the nanocage. The intensity and sign of the correlation are represented by the colored scale bar.

Using the averaged form factor (solid line in Figure 8), we compared the averaged theoretical intensity of the cage with the experimental data. As already mentioned in the previous work,²⁰ in the experimental solution, some aggregation occurs. The scattering at higher q is dominated by the scattering of the single cage,²⁰ and therefore, in order to compare the simulation data with the single cage scattering, some points of the data set at low q were omitted.

The simulation results are in good agreement with the experimental data, as shown in Figure 9. The scattering from the random component has an R_G value of 4 ± 1 nm and can probably be attributed to random parts of some nonperfectly assembled cages. The difference in the position of the oscillations after 0.40 nm^{-1} indicates that the average size of the cages in the SAXS sample is slightly larger than the structures obtained by MD, likely because of the nonperfect assembly of some of the cages.

CONCLUSION

The results obtained in this work demonstrate that the DNA double helices, composing the nanocage structure, are very stable (Tables 1 and 2) and that the

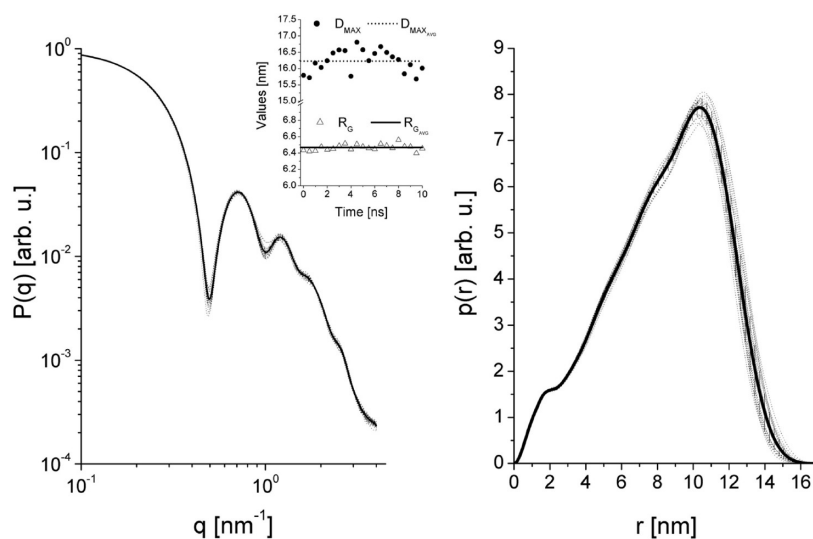


Figure 8. Theoretical scattering form factor (right) and pair distance distribution function (left) for the 20 MD extracted from the trajectory every 0.5 ns. The solid lines in both graphs are the average curve, and the error bars are the standard deviations. The inset shows the values of the radius of gyration (R_G) and maximum dimension (D_{MAX}) for the model obtained in each of the 20 configurations.

thymidine strands give a significant contribution to the organization of the scaffold geometry. The average structure obtained from the MD simulations is in good agreement with the experimental SAXS data for DNA cages in solution, some deviation occurring only in the position of the oscillations after 0.40 nm^{-1} and is likely due to a nonperfect assembly of some of the cages in the experimental solution.

The total rmsd (Figure 2) and the gyration radius (Figure 3) show that the starting truncated octahedron geometry, also if slightly distorted, is maintained along the entire trajectory. The comparison between the rmsd values of the double helices (Figure 1 of Supporting Information) and rmsd values of the single thymidine

TABLE 3. Size of the Simulated System^a

total atoms	392955
DNA atoms	19080
bases	600
water molecules	124425
Na^+ ions	600
simulation box side X (Å)	171
simulation box side Y (Å)	158
simulation box side Z (Å)	161
saved configurations	24000

^aSize, box dimensions, and number of damped configurations of the simulated system.

TABLE 4. System Thermalization Schemes^a

time (ps) ^b	procedure ^c	number of steps and ΔT	position restraint value ^d (kcal/mol Å)
0	EM1	30000	500 (all the nanocage)
12.5	MD1	25000 of 0.5 fs	500 (all the nanocage)
0	EM2	15000	500 (double helices only)
25.0	MD2	25000 of 1.0 fs	500 (double helices only)
0	EM3	10000	20 (all the nanocage)
40.0	MD3	20000 of 2.0 fs	no position restraints

^aThermalization scheme of the simulated system. ^bExecution time. ^cEM indicates an energy minimization procedure and MD a molecular dynamics procedure. ^dValues of used position restraints.

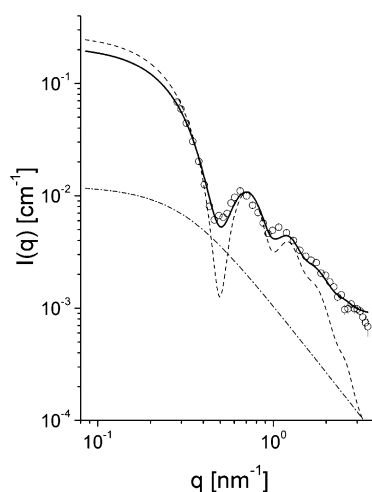


Figure 9. Comparison of the MD simulation results and the experimental SAXS data. Circles: experimental SAXS data. Solid line: scattering intensity calculated for the MD cages using formula 2. Dashed line: scattering from the MD cages without random component. Dashed-dotted line: scattering from random component.

strands (Figure 2 of Supporting Information) indicates that, in the global structure, the larger displacement is experienced by the thymidine strands. The local stability of every double helix is confirmed by the low rmsf values of the bases (Figure 3 of Supporting Information) and by the constancy of DNA helix geometrical parameters that are quite close to the typical B-DNA structure parameters (Table 1). The only parameter deviating from a typical B-DNA structure is the slide parameter that is related to the relatively large curvature observed in the DNA double helices (Table 2). The curvature is likely due to the constraints over the helices generated by the closed octahedral cage and by the stacking of the thymidines that collapse, one over the other, to

maximize the buried hydrophobic area, as shown in Figure 5. The main global motion evidenced by the PCA analysis (Figure 4 and Supporting Information movie file) indicates a small contraction of the cage, in line with the negative correlation displayed by the thymidine strands or the helices' strand not directly linked (Figure 7).

As a final result derived from the simulations, the global nanocage scaffold undergoes a contraction and the length of the thymidine strands seems to be the crucial aspect in the modulation of the nanocages' stability. In this context, we propose that decreasing the number of the thymidines would confer a higher rigidity and stability to the DNA nanocage.

METHODS

Molecular Modeling. The DNA nanocage starting structure was built by molecular modeling using the program Sybyl (TRIPOS, <http://www.tripos.com/>) (Figure 1A). Prebuilt 12 DNA double helices (DH1–DH12), each composed by 18 base pairs, were placed to satisfy the truncated octahedron polyhedral geometry revealed by the SAXS analysis²⁰ (Figure 1B). The 12 double helices were connected by 24 thymidine single strands, each composed by seven thymidines, in random conformation. Initial unfavorable interactions between the double helices and the thymidine strands were removed by local minimization through the SYBYL ANNEAL module.

MD Simulation. The system topology was obtained with the AMBER 8.0 leap module³² and modeled with the all-atoms AMBER03 force field.^{33,34} The DNA nanocage was immersed in a truncated octahedral box filled with TIP3P water molecules³⁵ (Table 3), imposing a minimal distance between the solute and the box walls of 10.0 Å. The system was neutralized through the AMBER leap module, adding 600 Na⁺ ions in electrostatic favorable positions. The final system consisted of 392 955 atoms (see Table 3). Optimization and relaxation of the entire system was initially performed through energy minimization and MD simulation of the solvent and the ions, keeping the solute atoms constrained to their initial positions with a 500 kcal force constant. Thereafter, the thymidine strands were equilibrated through energy minimization and MD simulation, restraining the atoms of DNA double helices with a 500 kcal force constant. The whole solute was minimized imposing a 20 kcal force constant and finally simulated using MD for 40 ps with a 2.0 fs time step, without any restraint, at a constant temperature of 300 K using the Berendsen's method³⁶ and at a constant pressure of 1 bar. After this procedure (Table 4), the system was simulated for 12 ns.

Pressure and temperature coupling constants were 0.4 ps. The atomic positions were saved every 250 steps (0.5 ps) for the analysis. The system was simulated in periodic boundary conditions, using a cutoff radius of 9.0 Å for the nonbonded interactions and updating the neighbor pair list every 10 steps. The electrostatic interactions were calculated with the particle mesh Ewald method.^{37,38} The SHAKE algorithm³⁹ was used to constrain all bond lengths. The calculations were carried out at CASPUR (Inter Universities Consortium for Supercomputing Applications) Rome, Italy, using 64 cores on the MATRIX cluster composed by 258 nodes, each with two AMD Opteron quadcore CPU, for a total of 2064 cores.

Analyses. The gyration radius, the root-mean-square deviation (rmsd), and root-mean-square fluctuation (rmsf) analyses were carried out using the GROMACS MD package version 4.0.2 program.⁴⁰ The DNA curvature and the geometrical parameters were calculated using the program CURVES.⁴¹

The buried hydrophobic surface of each thymidine strand was computed taking into consideration only the

thymidine rings. The overall solvent-accessible surface (SAS) of each strand was computed by the formula

$$\text{overall strand SAS} = (7\text{TS} - \text{SS})/2 \quad (1)$$

where TS (thymidine surface) = SAS of a free thymidine ring, SS (strand surface) = SAS of the overall strand. Both TS and SS were calculated by iteratively using the naccess program⁴² on each trajectory frame.

The correlation map³¹ of each DNA backbone phosphorus atom was calculated using the g_covar utility of the GROMACS MD package version 4.0.2 program.⁴⁰

To simplify the complexity of the correlation map, the full oligonucleotide sequences composing the nanocage were divided into two elements considered as independent units, namely, the thymidine single strands and the single strands forming the double helices. The correlation reported on the map refers to the correlation over the entire elements.

Small-Angle X-ray Scattering. The obtained MD model was compared with experimental SAXS data from a previous publication.²⁰ The SAXS results were obtained on laboratory-based SAXS equipment located at the Department of Chemistry in the University of Aarhus.⁴³ The experiments were carried out on self-assembled DNA cage structures with the same characteristics as the ones simulated. The scattering data are given as the intensity versus the momentum transfer modulus, q ($q = 4\pi \sin \theta/\lambda$, where 2θ is the scattering angle and λ is the X-ray wavelength).

The comparison with experimental data was done by scaling the theoretical intensity obtained from the MD simulation models to the experimental data using an overall scale factor. It turned out that the agreement between simulation and experiment was significantly improved if a contribution describing a disordered random component was included together with a constant background term:

$$I(q) = S_{c1}P(q) + S_{c2}P_{\text{polym}}(q) + \text{Back} \quad (2)$$

where S_{c1} and S_{c2} are scale factors, $P(q)$ is the average form factor obtained from the MD models, $P_{\text{polym}}(q)$ is the a disordered random component, and Back is a constant background. $P_{\text{polym}}(q)$ was taken as the scattering from Gaussian chains:

$$P_{\text{polym}}(q) = \frac{2[\text{exp}(x) - 1 + x]}{x^2} \quad (3)$$

where $x = R_G^2 q^2$ and R_G is the average gyration radius of the disordered random component. The form factor $P(q)$ of the cages was calculated from the atomic coordinates obtained from the MD using the Debye formula:

$$P_{\text{model}}(q) = \frac{F_{\text{sphere}}(q, R_{\text{bead}})^2}{N^2} \sum_{ij=1}^N \frac{\sin(qr_{ij})}{qr_{ij}} \quad (4)$$

where $F_{\text{sphere}}(q, R_{\text{bead}})$ is the form factor of a sphere of radius R_{bead} , and r_{ij} is the distance between the centers of the i th and j th subunit. To speed up the calculations, we used only the C2* sequence to describe the DNA structure using $R_{\text{bead}} = 0.7$ nm, which we have already shown to be a reasonable approximation for the resolution of SAXS experiments.²⁰ The parameters were optimized using a least-squares procedure.⁴⁴

Acknowledgment. F.F.A. and B.R.K. acknowledge support provided by the Carlsberg Foundation and the Aase og Einar Danielsen's Foundation. The authors thank the CASPUR (Inter Universities Consortium for Supercomputing Applications) Rome, Italy, for the computing facilities and the support provided for the calculations.

Supporting Information Available: Figure 1: All-atoms rmsd of the 12 double helices (from DH1 to DH12). Figure 2: All-atoms rmsd of the 24 thymidine single strands connecting the 12 DNA double helices. The connections are indicated in the upper side of each panel. Figure 3: Average per nucleotide RMSF for each of the two strands, defined by the black and gray filled circles, of the 12 DNA double helices (from DH1 to DH12). Figure 4: Average per nucleotide rmsf of the 24 thymidine single strands, connecting the 12 DNA double helices. The connections are indicated in the upper side of each panel. Figure 5: Cumulative fluctuation as a function of the eigenvector index for the nanocage structure. Only the first 20 eigenvectors are reported. Figure 6: Graphs showing the projections of the first, second, and third principal components. Movie (MPEG format) representing the animation of the projections along the first eigenvector for the DNA nanocage. The DNA backbones of the eight filaments composing the DNA nanocage are represented by different colors. This video has been produced using the VMD program.⁴⁵ This material is available free of charge via the Internet at <http://pubs.acs.org>.

REFERENCES AND NOTES

- Seeman, N. C. DNA Nanotechnology: Novel DNA Constructions. *Annu. Rev. Biophys. Biomol. Struct.* **1998**, *27*, 225–248.
- Seeman, N. C. DNA in a Material World. *Nature* **2003**, *421*, 427–431.
- Seeman, N. C. DNA Enables Nanoscale Control of the Structure of Matter. *Q. Rev. Biophys.* **2005**, *38*, 363–371.
- Seeman, N. C. From Genes to Machines: DNA Nanomechanical Devices. *Trends Biochem. Sci.* **2005**, *30*, 119–125.
- Ding, B.; Seeman, N. C. Operation of a DNA Robot Arm Inserted into a 2D DNA Crystalline Substrate. *Science* **2006**, *314*, 1583–1585.
- Andersen, F. F.; Andersen, K. E.; Kusk, M.; Fröhlich, R. F.; Westergaard, O.; Andersen, A. H.; Knudsen, B. R. Recombinogenic Flap Ligation Mediated by Human Topoisomerase I. *J. Mol. Biol.* **2003**, *330*, 235–246.
- Liao, S.; Mao, C.; Birktoft, J. J.; Shuman, S.; Seeman, N. C. Resolution of Undistorted Symmetric Immobile DNA Junctions by Vaccinia Topoisomerase I. *Biochemistry* **2004**, *43*, 1520–1531.
- Lee, J.; Tonzuka, T.; Jayaram, M. Mechanism of Active Site Exclusion in a Site-Specific Recombinase: Role of the DNA Substrate in Conferring Half-of-the-Sites Activity. *Genes Dev.* **1997**, *11*, 3061–3071.
- Winfrey, E.; Liu, F. R.; Wenzler, L. A.; Seeman, N. C. Design and Self-Assembly of Two-Dimensional DNA Crystals. *Nature* **1998**, *394*, 539–544.
- Yan, H.; Park, S. H.; Finkelstein, G.; Reif, J. H.; LaBean, T. H. DNA-Templated Self-Assembly of Protein Arrays and Highly Conductive Nanowires. *Science* **2003**, *301*, 1882–1884.
- Malo, J.; Mitchell, J. C.; Venien-Bryan, C.; Harris, J. R.; Wille, H.; Sherratt, D. J.; Turberfield, A. J. Engineering a 2D Protein–DNA Crystal. *Angew. Chem., Int. Ed.* **2005**, *44*, 3057–3061.
- Rinker, S.; Liu, Y.; Yan, H. Two-Dimensional LNA/DNA Arrays: Estimation the Helicity of LNA/DNA Hybrid Duplex. *Chem. Commun.* **2006**, *25*, 2675–2677.
- Rothmund, P. W. K. Folding DNA to Create Nano-Scale Shapes and Patterns. *Nature* **2006**, *440*, 297–302.
- Chen, J. H.; Seeman, N. C. Synthesis from DNA of a Molecule with the Connectivity of a Cube. *Nature* **1991**, *350*, 631–633.
- Zhang, Y.; Seeman, N. C. The Construction of a DNA Truncated Octahedron. *J. Am. Chem. Soc.* **1994**, *116*, 1661–1669.
- Shih, W. M.; Quispe, J. D.; Joyce, G. F. A 1.7-Kilobase Single-Stranded DNA That Folds into a Nanoscale Octahedron. *Nature* **2004**, *427*, 618–621.
- Goodman, R. P.; Schaap, A. T.; Tardin, C. F.; Erben, C. M.; Berry, R. M.; Schmidt, C. F.; Turberfield, A. J. Rapid Chiral Assembly of Rigid DNA Building Blocks for Molecular Nanofabrication. *Science* **2005**, *310*, 1661–1665.
- Erben, C. M.; Goodman, R. P.; Turberfield, A. J. A Self-Assembled DNA Bipyramid. *J. Am. Chem. Soc.* **2007**, *6*, 6992–6993.
- Aldaye, F. A.; Sleiman, H. F. Modular Access to Structurally Switchable 3D Discrete DNA Assemblies. *J. Am. Chem. Soc.* **2007**, *129*, 13376–13377.
- Andersen, F. F.; Knudsen, B.; Oliveira, C. L.; Fröhlich, R. F.; Krüger, D.; Bungert, J.; Agbandje-McKenna, M.; McKenna, R.; Juul, S. Assembly and Structural Analysis of a Covalently Closed Nano-Scale DNA Cage. *Nucleic Acids Res.* **2008**, *36*, 1113–1119.
- Maiti, P. K.; Pascal, T. A.; Vaidehi, N.; Goddard, W. A., III. The Stability of Seeman JX DNA Topoisomers of Paranemic Crossover (PX) Molecules as a Function of Crossover Number. *Nucleic Acids Res.* **2004**, *32*, 6047–6056.
- Maiti, P. K.; Pascal, T. A.; Vaidehi, N.; Heo, J.; Goddard, W. A., III. Atomic-Level Simulations of Seeman DNA Nanostructures: the Paranemic Crossover in Salt Solution. *Biophys. J.* **2006**, *90*, 1463–1479.
- Maiti, P. K.; Pascal, T. A.; Goddard, W. A., III. Understanding DNA Based Nanostructures. *J. Nanosci. Nanotechnol.* **2007**, *7*, 1712–1720.
- Lankas, F.; Lavery, R.; Maddocks, J. H. Kinking Occurs during Molecular Dynamics Simulations of Small DNA Minicircles. *Structure* **2006**, *14*, 1527–1534.
- Harris, S. A.; Laughton, C. A.; Liverpool, T. B. Mapping the Phase Diagram of the Writhe of DNA Nanocircles Using Atomistic Molecular Dynamics Simulations. *Nucleic Acids Res.* **2007**, *36*, 21–29.
- Garcia, A. E. Large-Amplitude Nonlinear Motions in Proteins. *Phys. Rev. Lett.* **1992**, *68*, 2696–2699.
- Falconi, M.; Oteri, F.; Eliseo, T.; Cicero, D. O.; Desideri, A. MD Simulations of Papillomavirus DNA–E2 Protein Complexes Hints at a Protein Structural Code for DNA Deformation. *Biophys. J.* **2008**, *95*, 1108–1117.
- Chillemi, G.; Falconi, M.; Amadei, A.; Zimatore, G.; Desideri, A.; Di Nola, A. The Essential Dynamics of Cu, Zn Superoxide Dismutase: Suggestion of Inter-Subunit Communication. *Biophys. J.* **1997**, *73*, 1007–1018.
- Arcangeli, C.; Bizzarri, A. R.; Cannistraro, S. Concerted Motions in Copper Plastocyanin and Azurin: An Essential Dynamics Study. *Biophys. Chem.* **2001**, *90*, 45–56.
- Hess, B. Convergence of Sampling in Proteins Simulations. *Phys. Rev. E* **2002**, *65*, 31910–31920.
- McCammon, J. A.; Harvey, S. C. Short Time Dynamics. *Dynamics of Proteins and Nucleic Acids*; Cambridge University Press: New York, 1987; pp 79–116.
- Case, D. A.; Cheatham, T. E., III; Darden, T.; Gohlke, H.; Luo, R.; Merz, K. M.; Onufriev, A., Jr.; Simmerling, C.; Wang, B.; Woods, R. The AMBER Biomolecular Simulation Programs. *J. Comput. Chem.* **2005**, *26*, 1668–1688.
- Duan, Y.; Wu, C.; Chowdhury, S.; Lee, M. C.; Xiong, G.; Zhang, W.; Yang, R.; Cieplak, P.; Luo, R.; Lee, T. A. Point-Charge Force Field for Molecular Mechanics Simulations of Proteins. *J. Comput. Chem.* **2003**, *24*, 1999–2012.
- Ponder, J. W.; Case, D. A. Force Fields for Protein Simulations. *Adv. Protein Chem.* **2003**, *66*, 27–85.

35. Jorgensen, W. L.; Chandrasekhar, J.; Madura, J. D.; Impey, R. W.; Klein, M. L. Comparison of Simple Potential Functions for Simulating Liquid Water. *J. Chem. Phys.* **1983**, *79*, 926–935.
36. Berendsen, H. J. C.; Postma, J. P. M.; van Gusteren, W. F.; Di Nola, A.; Haak, J. R. Molecular Dynamics with Coupling to an External Bath. *J. Comput. Phys.* **1984**, *81*, 3684–3690.
37. Darden, T.; York, D.; Pedersen, L. Particle Mesh Ewald an $N \cdot \log(n)$ Method for Ewald Sums in Large Systems. *J. Chem. Phys.* **1993**, *98*, 10089–10092.
38. Cheatham, T. E.; Miller, J. L.; Fox, T.; Darden, T. A.; Kollman, P. A. Molecular Dynamics Simulation on Solvated Biomolecular Systems: The Particle Mesh Ewald Method Leads to Stable Trajectories of DNA, RNA and Proteins. *J. Am. Chem. Soc.* **1995**, *117*, 4193–4194.
39. Ryckaert, J. P.; Ciccotti, G.; Berendsen, H. J. C. Numerical Integration of the Cartesian Equations of Motion of a System with Constraints: Molecular Dynamics of n -Alkanes. *J. Comput. Phys.* **1977**, *23*, 327–341.
40. Hess, B.; Kutzner, C.; van der Spoel, D.; Lindahl, E. GROMACS 4: Algorithms for Highly Efficient, Load-Balanced, and Scalable Molecular Simulation. *J. Chem. Theory Comput.* **2008**, *4*, 435–447.
41. Lavery, R.; Sklenar, H. Defining the Structure of Irregular Nucleic Acids: Conventions and Principles. *J. Biomol. Struct. Dyn.* **1989**, *6*, 655–667.
42. Hubbard, S. J.; Thornton, J. M. *NACCESS*; Department of Biochemistry and Molecular Biology, University College London, 1993.
43. Pedersen, J. S. A Flux- and Background-Optimized Version of the NanoSTAR Small-Angle X-ray Scattering Camera for Solution Scattering. *J. Appl. Crystallogr.* **2004**, *37*, 369–380.
44. Pedersen, J. S. Analysis of Small-Angle Scattering Data from Colloids and Polymer Solutions: Modeling and Least-Squares Fitting. *Adv. Colloid Interface Sci.* **1997**, *70*, 171–210.
45. Humphrey, W.; Dalke, A.; Schulten, K. VMD—Visual Molecular Dynamics. *J. Mol. Graph.* **1996**, *14*, 33–38.